Ion escape from Mars as a function of solar wind conditions: A statistical study

Hans Nilsson [a,*], Ella Carlsson [a], David A. Brain [b], Masatoshi Yamauchi [a], Mats Holmström [a], Stas Barabash [a], Rickard Lundin [a], Yoshifumi Futaana [a]

[a] Swedish Institute of Space Physics, Box 812, 981 28 Kiruna, Sweden
[b] Space Science Laboratory, University of California, Berkeley, CA 94720, USA

ABSTRACT

The influence of solar EUV and solar wind conditions on ion escape at Mars is investigated using ion data from the Aspera-3 instrument on Mars Express, combined with solar wind proxy data obtained from the Mars Global Surveyor (MGS) spacecraft. A solar EUV flux proxy based on data from the Earth position, scaled and shifted in time for Mars, is used to study relatively long time scale changes related to solar EUV variability. Data from May 2004 until November 2005 has been used. A clear dependence on the strength of the subsolar magnetic field as inferred from MGS measurements is seen in the ion data. The region of significant heavy ion flows is compressed and the heavy ion flux density is higher for high subsolar magnetic field strength. Because of the difference in outflow area, the difference in estimated total outflow is somewhat less than the difference in average flux density. We confirm previous findings that escaping planetary ions are mainly seen in the hemisphere into which the solar wind electric field is pointed. The effect is more pronounced for the high subsolar magnetic field case. The average ion motion has a consistent bias towards the direction of the solar wind electric field, but the main motion is in the antisunward direction. The antisunward flow velocity increases with tailward distance, reaching above 100 km s^{-1} at 2 to 3 martian radii downtail from Mars for O$^+$ ions. Different ion species reach approximately the same bulk flow energy. We did not find any clear correlation between the solar EUV flux and the ion escape distribution or rate, probably because the variation of the solar EUV flux over our study interval was too small. The results indicate that the solar wind and its magnetic field directly interacts with the ionosphere of Mars, removing more ions for high subsolar magnetic field strength. The interaction region and the tail heavy ion flow region are not perfectly shielded from the solar wind electric field, which accelerates particles over relatively large tail distances.

© 2009 Elsevier Inc. All rights reserved.

1. Introduction

When the solar wind flows around non-magnetized planets like Mars, three important boundaries will form, the bow shock, the magnetic pile up boundary, also called the induced magnetosphere boundary (IMB), and finally an inner boundary which may be of the form of an ionopause. Solar wind magnetic field lines pile up against the effective obstacle to the solar wind flow, forming a magnetic pile up region between the outer magnetic pile-up boundary (MPB, assumed to be the same as the IMB in this text) and the inner boundary. On average there must be a pressure balance between the outer force, the solar wind dynamic pressure, and an inner force. In the magnetic pile-up region there may be a gradual transition between different pressure terms which in the end must be balanced by an inner force at the low altitude boundary of the interaction region. If the inner force is the plasma pressure of the ionosphere a proper ionopause is formed. If the ionospheric pressure is too low

the solar wind magnetic field may penetrate into the ionosphere, and there will be a partially magnetized ionosphere. For Venus it has been shown that both cases exist (Luhmann, 1990), depending on the level of the solar wind pressure. Similar studies have not been available from Mars, but recently Dubinin et al. (2008) were able to study the pressure balance at Mars through the use of the MARSIS sounder in complement to the ASPERA-3 plasma instrument ion and electron measurements. They found that the ionosphere of Mars was partially magnetized for the cases studied. The behavior of all these boundaries in response to changing solar conditions may affect the net escape rate of ions for different phases of the solar cycle as well as for different phases of the age of the Sun.

The average bow shock position has been reported to be fairly stationary regardless of solar EUV fluxes (Vignes et al., 2002; Trotignon et al., 2006), based on Phobos 2 and the more recent Mars Global Surveyor (MGS) measurements. The individual variability is large, with no clear dependence on solar activity and solar wind ram pressure (Trotignon et al., 2006).

The magnetic pile up boundary (MPB) has been most studied by the magnetometer and electron spectrometer on the MGS space-

* Corresponding author. Fax: +46 98079050.
E-mail address: hans.nilsson@irf.se (H. Nilsson).

craft. Brain et al. (2005) summarizes most of the results from the MGS measurements; that the position of the MPB has a strong seasonal asymmetry, being lower for northern summer, a clear dependence on subsolar magnetic field strength, with stronger magnetic field pushing the MPB closer to the planet, some dependence on the solar wind magnetic field draping angle and a clear dependence on the presence of crustal magnetic anomalies, with strong anomalies raising the altitude of the MPB. A search for a correlation between the presence of heavy (planetary origin) ion beams and crustal magnetic fields did not show any relation (Nilsson et al., 2006). The ions studied where of energies greater than 300 eV, so it is not unlikely that the crustal magnetic anomalies were too small compared to the gyro radii of the ions to have any significant influence. Instead it has become clear that the main factor controlling the position of outflowing ions, at least with energies above a few 100 eV, is the direction of the solar wind electric field. Fedorov et al. (2006), Dubinin et al. (2006), Barabash et al. (2007) clearly demonstrate how the largest heavy ion fluxes are seen in the hemisphere into which the solar wind electric field is pointed. Dubinin et al. (2006) showed a number of examples where the ion energy increased steeply with altitude, consistent with a more or less direct acceleration by the solar wind electric field. This implies that, at least on occasions, the solar wind can penetrate deep into the martian magnetosphere. Based on Phobos measurements Dubinin et al. (1993) showed that planetary ions where typically accelerated to approximately the same energy per charge, regardless of their mass. The ions reached about the energy of the solar wind protons. This indicates an acceleration in an electric field, and is different from typical pick up processes which should give the same velocity to different ion species. Therefore the penetration of the solar wind electric field may be an important factor determining the acceleration of heavy ions up to and beyond escape velocity. The volumes affected by the solar wind electric field, and the ion densities in these regions, may be equally important in determining the net escape rate.

Ion escape at Mars has mainly been studied by the Phobos 2 mission and more recently by the Mars Express mission. The former mission provided data for high solar activity and estimated escape rates ranged from 5×10^{24} s^{-1} (Verigin et al., 1991) up to 3×10^{25} s^{-1} (Lundin et al., 1990). Much of the uncertainty in these high solar activity estimates comes from assumptions about the area of the outflow and the relatively short measurement period. The escape rates determined based on Mars Express measurements were up to two orders of magnitude lower, 3×10^{23} s^{-1} (Barabash et al., 2007). The initial Mars Express data did not incorporate any ions with energy below 30 eV. With a recent patch to the on-board software it is now possible to get reliable estimates down to energies where the spacecraft potential starts to be a problem, i.e. at about 10 eV or so. Lundin et al. (2008b) used the new low energy ion data to determine how much the low energy escape adds to the net escape and found that the total escape rates for low solar activity reached about 3×10^{24} s^{-1} for the period June 2007 to March 2008. The more energetic ion beams were estimated to contribute 7.7×10^{23} s^{-1} for this time period, which is about twice the estimate from the time period 1 May 2004 to 30 May 2006 used by Barabash et al. (2007). The low energy ion fluxes decreased with downtail distance, whereas the high energy ions increased. This is consistent with some of the low energy ions being accelerated, but clearly not all of them.

Lundin et al. (2008a) also examined the solar wind forcing of ion escape based on 42 selected orbits with Mars Express ion data. They looked at short time changes, and tried to estimate how the area and flux density of the outflow was affected by changing solar and solar wind conditions for several individual orbits. They found that solar EUV related forcing and solar wind pressure forcing were equally important for the net escape rate. Futaana et al. (2008) reported observations of the ion escape from a large solar energetic particle event taking place in December 2006. They found that the net escape rate was almost an order of magnitude enhanced during the event. They suggested that the effect of the energetic particles could be compared to that of higher solar EUV fluxes during solar maximum, and therefore the measurements indicate a significant dependence of the total outflow on solar EUV forcing.

There is clearly room to improve both our understanding of the processes leading to ion escape at Mars, and to further investigate the total ion escape rate. Here we contribute to this by an empirical study of the effect of the solar wind on the ion distribution, acceleration and rate of escape at Mars. We use the subsolar magnetic field strength and draping angle proxies from Mars Global Surveyor and ion data from Mars Express. This is complemented with a proxy for the solar EUV flux at Earth, scaled and shifted in time for Mars. We use data from May 2004 until November 2005.

2. Instrument description

We use data from the Ion Mass Analyzer (IMA), part of the ASPERA-3 plasma instrument package on the Mars Express spacecraft (Barabash et al., 2006, see for details). IMA has an energy coverage of about 10 eV to 36 keV, but for the data we use the lower energy range is rather 30 eV. The intrinsic field-of view of IMA is 4.5° by 360° in the spacecraft X–Z plane (see e.g. Barabash et al. (2006), their Fig. 37 for a description of the spacecraft coordinate system and Nilsson et al. (2006) their Fig. 1 for a schematic description of the IMA field-of-view in the spacecraft coordinate system). An electrostatic entrance deflection system brings particles from $\pm 45°$ from the viewing plane of the instrument into the detector, thus providing a limited 3D view. Part of this 3D view is obstructed by the spacecraft. The instrument is stepped through 96 energy levels in 12 s, and through 16 electrostatic entrance deflection levels (corresponding to the $\pm 45°$ angular interval) in a total of 192 s. At the lowest energies, below 50 eV, the electrostatic entrance deflection has insufficient resolution to properly guide the ions into the instrument. From June 2007 the instrument performance has also been further adjusted based on in-flight calibrations and now provides good data down to about 10 eV. Since May 2007, no entrance deflection is used below 50 eV, and the instrument thus has a 2D view at these energies. Such a 2D mode has also been used at all energies, in particular from December 2005 and during a significant part of 2006. This improves time resolution but limits the angular coverage. We have therefore opted to omit the data from December 2005 and throughout 2006 for the study reported here. The data without entrance deflection deserves some special attention and we have chosen to present the results of one coherent data set with 3D data here. Unfortunately there is no overlap between the new IMA data with good coverage at low energy and MGS measurements. The latter stopped in early November 2006.

The IMA instrument determines the mass of the ions through a magnetic deflection system and a micro-channel plate based position detection system. This system is low power, simple and robust, but gives limited mass resolution. The peaks in the mass spectrum caused by O^+, O_2^+ and CO_2^+ partially overlap, but can be separated through fitting of response functions corresponding to the three species (Carlsson et al., 2006). A more severe problem is that intense proton fluxes may contaminate mass channels corresponding to other species. This signal created by intense proton fluxes is quite characteristic and can to a large extent be automatically detected and accounted for. It is however clear from our data that some contamination remains after the automatic cleaning process. We have therefore opted to use heavy ion data only when the proton and alpha flux is low. There may therefore be further ion escape corresponding to picked up ions in the magnetosheath and solar wind. Our study does not include such ions.

To describe varying solar wind conditions we have used two proxies based on MGS magnetometer data, the subsolar magnetic field strength and the solar wind draping angle. The subsolar magnetic field strength proxy is based on MGS magnetic field measurements taken at solar zenith angles (SZA) less than 110° and taken well away from strong or moderate crustal magnetic fields (Brain et al., 2005). The data is fitted to a cos(SZA) function and extrapolated to the subsolar point. This is considered to be a proxy for the subsolar magnetic field. The solar wind draping angle is estimated in a similar way, using data from 50° to 60° N planetary latitude on the dayside (Brain et al., 2006). This draping angle is a function of the solar wind clock angle and we use it as a proxy to calculate the solar wind electric field direction. However the draping angles show a different distribution from that of the interplanetary magnetic field (IMF) clock angle, clustering around smaller angular ranges (see Brain et al. (2006) for more details). The proxy does correspond well to the sector of the solar wind magnetic field, and therefore provides at least an approximate proxy of the IMF clock angle. Both MGS measurements based proxies are orbit based and thus of rather low temporal resolution. They are therefore best suited for rather large statistical studies. Finally, we have used solar EUV flux (F10.7 cm) proxies for Earth scaled with solar distance as r^{-2}, and shifted in time (assuming a 26 day solar rotation) for Mars (Mitchell et al., 2001).

3. Results

3.1. Data set

We have used all Mars Express IMA data from May 2004 until November 2005. This represents most of the data when IMA was used in standard 3D mode while MGS was still operational. We have removed all heavy ion data when the H⁺ flux or He²⁺ flux was above 10^9 m⁻² s⁻¹. This will not remove much data as it is well established that the solar wind proton flux decrease significantly at the induced magnetopause/magnetic pile-up boundary, see e.g. Sauer et al. (1994) for an introduction to this subject. However one should still note that our data describes heavy ion flow in regions with low solar wind origin ion fluxes. We show the proton flux in Fig. 1 to illustrate that the induced magnetospheric cavity in the solar wind does indeed occur where we expect it to be. Fig. 1 is divided into two panels, one for high (upper panel) and one for low subsolar magnetic field (lower panel). The x axis of Fig. 1 shows the Mars-Solar-Orbital (MSO) x coordinate (positive towards the Sun) in martian radii (of 3393 km), the y axis shows the distance away from the x axis ($\sqrt{Y_{MSO}^2 + Z_{MSO}^2}$) in R_M. The color scale indicates the logarithm of the H⁺ flux in units of m⁻² s⁻¹. Data on the outer edges, in particular towards positive x values, have poor statistics and show some outliers. These are not significant but we have chosen to keep them in order to show the data in the way it comes out of our analysis. The number of samples is shown in Fig. 2. The upper panel of Fig. 2 shows the total number of samples in each bin, the lower panel shows the number of samples with proton and alpha fluxes below a threshold of 10^9 part m⁻², i.e. allowing for detection of heavy ions.

We have binned the data as above and below the median subsolar magnetic field and median solar EUV flux. This is because we cannot, as in a laboratory experiment, vary only one parameter at a time. By using just two broad categories, above and below median, we maximize the likelihood that the contribution from all other independent variables is the same for the two data sets.

High solar wind magnetic field is defined as above the median for our measurements, i.e. above 41 nT. The H⁺ fluxes are on average 4 times higher, and the proton drop off occur closer to the planet for high subsolar magnetic field strength. Thus on average
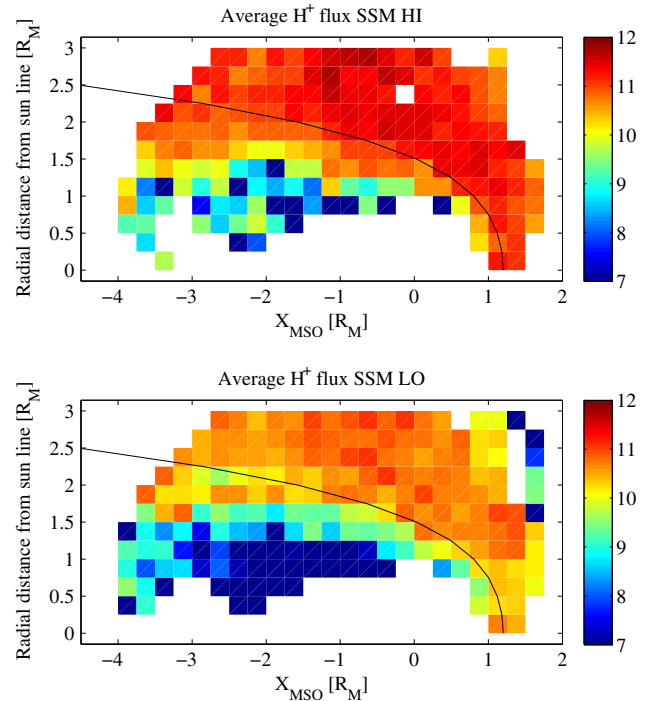

Fig. 1. The color scale shows the logarithm of average flux of protons [m⁻² s⁻¹] for high subsolar magnetic field strength (upper panel) and low subsolar magnetic field strength (lower panel). The median value of 41 nT subsolar magnetic field strength was used to divide the two data sets. The x axis shows X_{MSO} distance, positive towards the Sun, with Mars center at the origin, in units of martian radii (R_M). The y axis shows the radial distance from the X_{MSO} line, i.e. $\sqrt{Y_{MSO}^2 + Z_{MSO}^2}$ in R_M. The thin black line denotes the nominal position of the induced magnetosphere boundary.
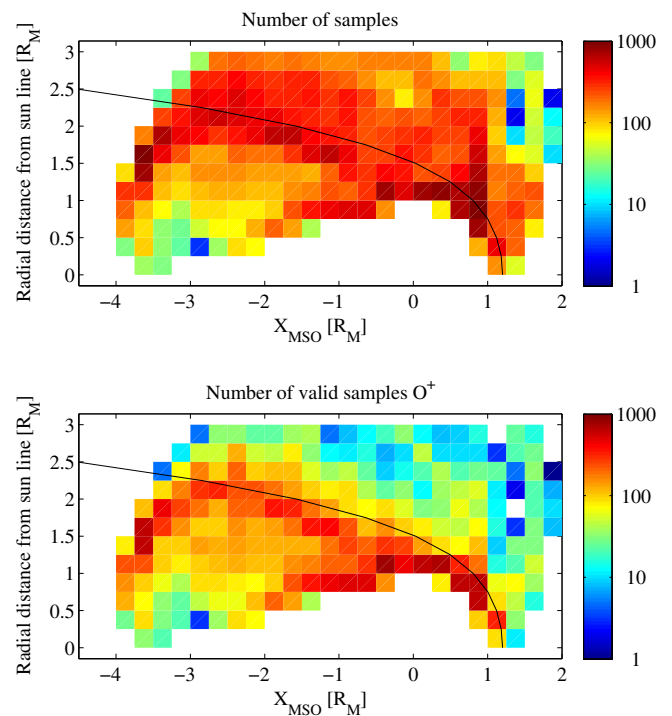

Fig. 2. The color scale shows the logarithm of the number of samples for all data (upper panel) and with proton and alpha particle flux below a threshold of 10^9 part m⁻² (lower panel). The axis are the same as for Fig. 1.
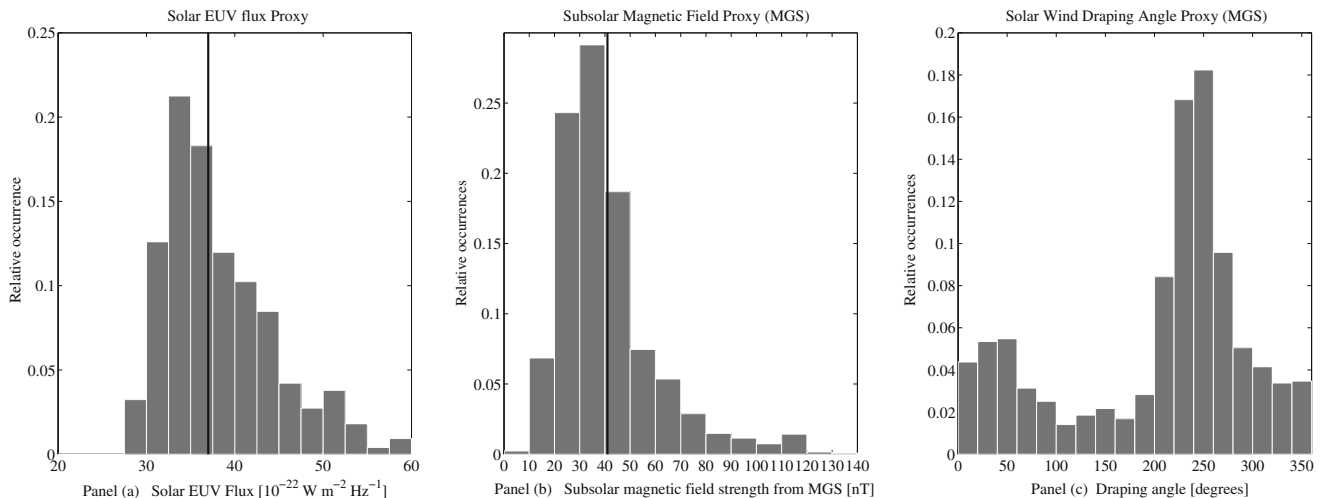
Fig. 3. Histograms of the different proxy values for our data set. Panel (a): Solar EUV flux proxy, based on F10.7 cm solar EUV proxy for Earth, scaled and shifted in time for Mars. The median value of 37 is shown with a vertical black line. Panel (b): Subsolar magnetic field strength proxy derived from MGS measurements. The median value of 41 nT is shown with a vertical black line. Panel (c): Solar wind draping angle as determined from MGS measurements.

the subsolar magnetic field from MGS does indeed correspond to higher solar wind fluxes as we would expect. The shape of the proton drop off follows the nominal shape for the induced magnetosphere boundary (thin black line) close to the planet, but there is significant deviation further back in the tail. The nominal IMB was derived from another data set and a different phase of the solar cycle (Phobos 2 at solar maximum, see Kallio (1996) for details), so this may indeed reflect a difference in the shape of the IMB as compared to the model IMB, or an intrusion of solar wind origin plasma. Though this is indeed an interesting topic we leave the details of this for a future study.

The IMA coverage in the solar wind is uneven, and a plot of solar wind fluxes as a function of the subsolar magnetic field strength gives a rather large scatter (not shown). However the previous result indicates that on average the solar wind flux and the subsolar magnetic field strength behaves in a similar way. IMA data from outside the nominal IMB, when solar wind fluxes dominates, can therefore give an estimate of the prevailing solar wind conditions for each orbit. It will be a low time resolution estimate, just like the MGS subsolar magnetic field strength value, with one or two values per orbit. Dividing the data set after above and below median solar wind flux gives a similar result to the subsolar magnetic field case (see Section 3.3). In the absence of MGS data the IMA proton data can therefore be used to order the data in the two broad categories we have used, above and below median solar wind flux.

We have calculated average fluxes of H^+, He^{2+}, O^+ and for the sum of the heavy ions in the mass range of O^+ to CO_2^+. For one of the dominant heavy ions, O^+, we also present moment calculations of the bulk velocity. The main flow is in the antisunward direction. Therefore we have also tried to add the criterion that the Sun direction should be within the unobstructed half of the 3D field-of-view of IMA. This is in order to see if some orbits with low counts were affected by the viewing geometry rather than low ion fluxes. This turned out to have only a minor effect on the average ion fluxes. The fluxes presented later are averages over the presented bin. The instantaneous flux density when ions are observed is typically higher. This is for example because of the dependence on the direction of the solar wind electric field which appears to control where ions are seen. Taking the average over many orbits, where no ions are detected in part of the orbits, allows us to take the uneven distribution of the ions into account. The occurrence frequency is then convolved into the average flux, which facilitates integrating over area to obtain total flux.

The distributions of the proxies we use are shown in Fig. 3, with vertical black lines indicating median values. Panel a shows the distribution of the solar EUV proxy, with a median of 37 and an average for the below median values of 33 and the above median values have an average of 43, in units of 10^{-22} W m^{-2} Hz^{-1}. This is a rather small spread of values, and we do not expect to be able to extrapolate to high solar activity conditions based on our range of solar EUV flux proxy values. For comparison, the scaled solar EUV flux for the MGS mapping period ranged up to a scaled flux of about 130. Panel b shows the distribution of subsolar magnetic field values, with a median of 41 nT, and an average below median of 29 nT and above median of 60 nT. Panel c finally shows the solar wind draping angle. As can be seen the distribution is uneven, with a clear peak around 250° and a smaller peak around 40°. This represents the distribution of the draped magnetic field as measured by MGS, it does not directly reflect the IMF clock-angle (Brain et al., 2006).

3.2. Influence of the solar EUV

The average O^+ fluxes sorted after high (upper panel) and low (lower panel) solar EUV are shown in Fig. 4. The logarithm of the flux density is shown by a color scale [m^{-2} s^{-1}]. Black arrows indicate the average bulk plasma velocity, with a scale of 500 km s^{-1} R_M. Note that statistics are typically poor in the outermost bins containing data. White indicates no valid data. It is important to note that the fluxes around Mars do not necessarily show cylindrical symmetry, more ions are seen in the hemisphere into which the solar wind electric field is pointed, see Section 3.4, as well as the simulation results summarized in the SWIM workshop model comparison study (Brain et al., 2008).

It is not possible to discern any relation between the average ion flux density and the solar EUV flux. Neither does the solar EUV flux significantly affect the shape and size of the region with significant oxygen ion flux density. The same is true for the total ion flow in the tail and the flow as function of Z_{MSE}, the direction of the solar wind electric field (not shown).

3.3. Influence of the subsolar magnetic field

The average O^+ fluxes sorted after high (upper panel) and low (lower panel) subsolar magnetic field strength (SSM) are shown in Fig. 5. The logarithm of the flux density is shown by a color scale
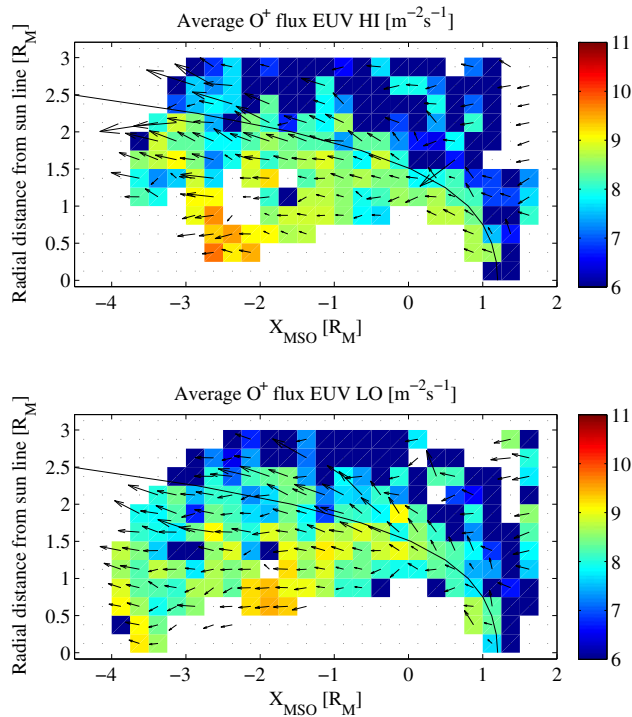
Fig. 4. The color scale shows the logarithm of average flux of O^+ [m^{-2} s^{-1}] for high solar EUV flux (upper panel) and low solar EUV flux (lower panel). The median value of the solar EUV flux of 37×10^{-22} W^{-1} m^{-2} Hz^{-1} was used to divide the two data sets. The axis are the same as for Fig. 1. Black arrows indicates the average ion bulk velocity, with a scale of 500 km s^{-1}/R_M.

Fig. 5. The color scale shows the logarithm of average flux of O^+ [m^{-2} s^{-1}] for high subsolar magnetic field strength (upper panel) and low subsolar magnetic field strength (lower panel). The median value of 41 nT subsolar magnetic field strength was used to divide the two data sets. The axis are the same as for Fig. 1. Black arrows indicates the average ion bulk velocity, with a scale of 500 km s^{-1}/R_M.

[m^{-2} s^{-1}]. The coordinate system is the same as for Fig. 4 One can see a clear relation between subsolar magnetic field strength and average flux density as well as the distribution of bins with significant flux density. For high subsolar magnetic field strength the induced magnetosphere is compressed and the average flux density within the IMB is higher. For low subsolar magnetic field we commonly see significant flux also outside the nominal IMB. To make really sure that this is not an artifact due to cross-talk from protons, as described in Section 2) we have re-run our code with a proton and alpha particle threshold of 10^3 m^{-2} s^{-1}, which means essentially no solar wind ions. The result remains the same. It is also worthwhile to once again investigate Fig. 2, where the statistical significance of the fluxes just outside the nominal IMB can be studied. The number of valid samples drop off, from several hundred samples per spatial bin inside the nominal IMB to several tens just outside, reflecting the typical proton flux distribution. Almost all valid samples outside the nominal IMB are for the low subsolar magnetic field strength case (not shown). At the same time the average proton flux shown in Fig. 1 does not seem to have a very different spatial distribution for the high and low subsolar magnetic field case. This implies that cases with low solar wind fluxes outside the nominal IMB occur sporadically and mainly for the low subsolar magnetic field strength case. In these cases we see significant heavy ion fluxes outside the nominal IMB. Note that these fluxes are not outside the instantaneous IMB because of our demand that the simultaneously observed proton flux should be low. The average O^+ ion flux as shown in Fig. 5 has been normalized with the total number of samples (upper panel of Fig. 2) to show the average flux over all measurements. The average flux outside the nominal IMB is therefore more significant than the number of valid heavy ion observations may imply.

Note that there are some outliers at $X_{MSO} = 1.5$ for low subsolar magnetic field. The statistics are very poor in this region so no significance should be given to these values. We have chosen to keep
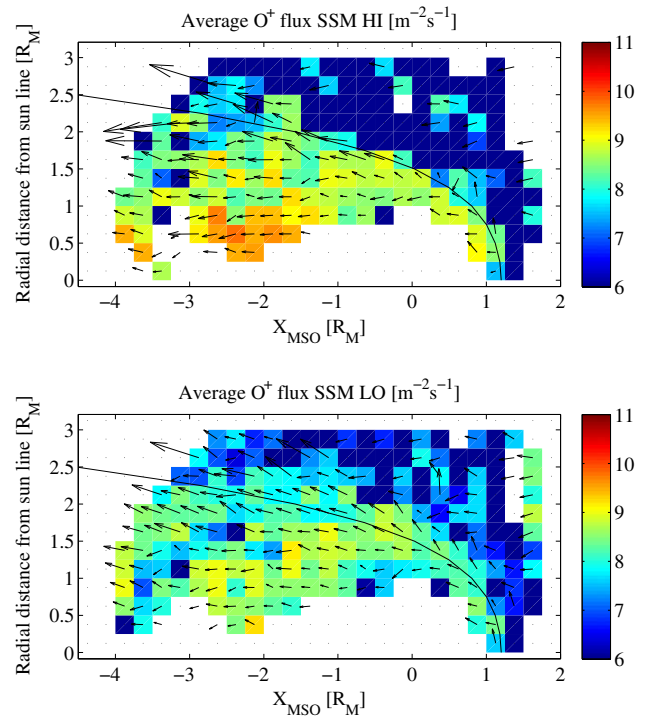
them in the plot in order to show the data as it comes out of our analysis. This is a region with strong waves at the proton gyro frequency (Brain et al., 2002). Such waves are consistent with solar wind pick up of Mars hydrogen exosphere, so there is reason to look further into this region, but that will have to be the subject of another study.

We complement the study of the influence of the subsolar magnetic field with a study of the influence of the solar wind flux as determined from the IMA data. Fig. 6 shows the same data as Fig. 5 but ordered after above (upper panel) and below (lower panel) median solar wind flux. The result is close to the same as for the subsolar magnetic field case, but a bit more pronounced. The average flux of planetary origin ions outside the nominal IMB for high solar wind flux is even lower than for high subsolar magnetic field. The average flux outside the nominal IMB is consistently somewhat higher for the low solar wind flux case than for the low subsolar magnetic field case.

The result presented in Figs. 5 and 6 indicates that as the subsolar magnetic field and solar wind flux increase, the area dominated by outflowing planetary ions decreases while the flux density increases. It is not obvious from the figures how the total outflow will be affected. We therefore show the net heavy ion outflow, ordered after subsolar magnetic field strength, in Fig. 7. We now use the total flux of heavy ions in the O^+ to CO_2^+ mass range. The data have first been binned into X_{MSO} and r bins as in Fig. 5. The average flux density and standard deviation of the flux have then been calculated for each bin. We use all bins, not just inside the nominal IMB, though this does not strongly affect the result. The average flux density has then been multiplied with the annular area corresponding to each bin. The standard deviations for each bin have been combined as for independent variables to get a variability of the total outflow for each tail distance. The error bars shown in Fig. 7 indicate the standard deviation divided by the square root
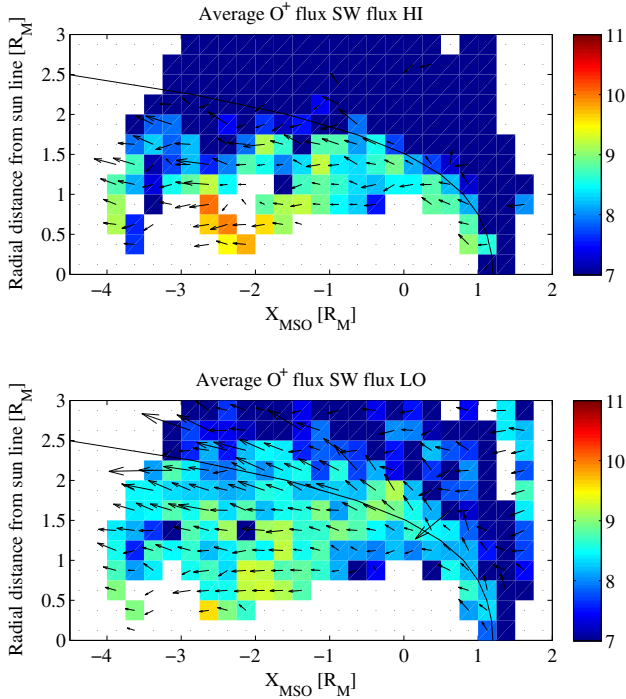
Fig. 6. The color scale shows the logarithm of average flux of O^+ [m^{-2} s^{-1}] for high solar wind flux (upper panel) and low solar wind flux (lower panel). The median value of 4×10^{10} m^{-2} s^{-1} solar wind flux density was used to divide the two data sets. The axis are the same as for Fig. 1. Black arrows indicates the average ion bulk velocity, with a scale of 500 km s^{-1}/R_M.
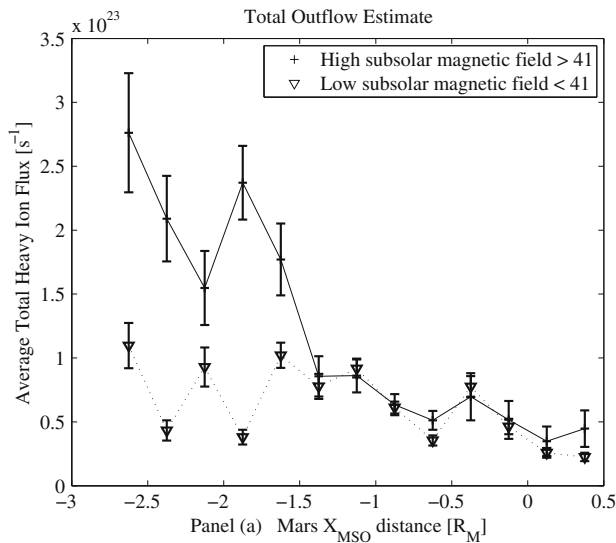

Fig. 7. The x axis shows X_{MSO} distance, positive towards the Sun, with Mars center at the origin, in units of martian radii (R_M). The y axis shows the total outflow of all heavy ions in the O^+ to CO_2^+ mass range [s^{-1}]. Short horizontal bars joined by a solid line indicate the high subsolar magnetic field case. Triangles joined by a dotted line indicate the low subsolar magnetic field case. Error bars indicate the 95% confidence interval for the mean of a normal distribution.

of the number of samples multiplied by 1.96. This would yield a 95% confidence interval for normally distributed data. The increase with tail distance is reasonable and indicates that more ions are accelerated into the instrument measurement range. The variability beyond 1.5 R_M tail distance, though larger than our uncertainty estimates, must be due to random fluctuations. This indicates that we under estimate the uncertainty, but we can still clearly see that

the net escape increases with tailward distance for the high subsolar magnetic field case. The total outflow we calculate is slightly lower than what was obtained in Barabash et al. (2007). The high solar wind pressure case yields the same total escape of 3×10^{23} s^{-1}, whereas the low solar wind pressure case of about 1×10^{23} s^{-1} yields a somewhat lower total escape. This is not due to the different data taking periods, using the same data period as in Barabash et al. (2007) yields just slightly higher escape rates in our analysis. The difference may come from stronger background subtraction and harder screening against possible proton contamination in our data set. This is likely to remove some real heavy ion data, but is necessary in order to make our comparison of different solar wind conditions trustworthy.

3.4. Influence of the solar wind electric field direction

We have calculated a solar wind electric field direction, Z_{MSE}, where MSE denotes a Mars–Sun-electric field direction coordinate system. X is from Mars center towards the Sun as in the MSO coordinate system, but Z is along the estimated solar wind electric field direction. Y_{MSE} complements a righthanded system. We have estimated the solar wind electric field direction based on the assumption that the draping angle estimated from MGS is the same as the interplanetary magnetic field clock angle, though this is not exactly true. The O^+ flux data are shown in Fig. 8. The logarithm of the flux density is shown by a color scale [m^{-2} s^{-1}]. The x axis shows the X_{MSO} axis, positive towards the Sun and with Mars center at the origin, and the y axis shows the Z_{MSE} axis, both in martian radii. Data have been integrated over all Y_{MSE} ranges. A black line shows the position of the nominal IMB. and black arrows show the average O^+ bulk velocity with a scale of 500 km s^{-1}/R_M. The upper panel shows the flux for high , the lower panel the flux for low subsolar magnetic field. An asymmetry can be discerned, with more flux in the $+Z_{MSE}$ hemisphere. The asymmetry is particularly clear for the high subsolar magnetic field case. The increase is less pronounced but still significant for the low subsolar magnetic field case. The hemispheric average flux density is 2 to 3 times higher in the hemisphere into which the estimated solar wind electric field is pointed. Note also that this is based on a low time resolution proxy. Any errors in the determination of the solar wind electric field direction will result in a smearing of the results. Therefore one must conclude that if the solar wind electric field estimate, with all its limitations, can sort the data this well, the solar wind electric field direction likely orders the heavy ion flux data very well.

The velocity in the Z_{MSE} direction appears to have a slight average shift upward in the direction of the electric field. To look at this in more detail we show in Fig. 9 the sunward velocity (upper panel) and the velocity in the direction of the solar wind electric field (lower panel), both in km s^{-1}. The tailward velocity increases from an initial value of about 70 km s^{-1} in the vicinity of Mars to about 120 km s^{-1} at 3 Mars radii down-tail distance. The velocity in the Z_{MSE} direction is smaller but consistently positive on average. This can be expected if the electric field is responsible for accelerating the particles, part of the motion would be in the direction of the field. It is not obvious that a penetrating solar wind electric field must be in the same direction inside the draped field lines as in the solar wind, but on a large scale it should be roughly in the same direction. The main reason for this is that the distribution of the ions is according to this direction of the external solar wind electric field, and the direction we use was inferred from MGS measurements relatively close to the planet (400 km altitude in the dayside). By the ratio of the velocity in the Z_{MSE} direction and the tailward velocity, together with the increase in bulk flow energy with tail distance we can make an estimate of a penetrating solar wind electric field which affects the particles, assuming all the work done on the particles is represented by the electric field force and
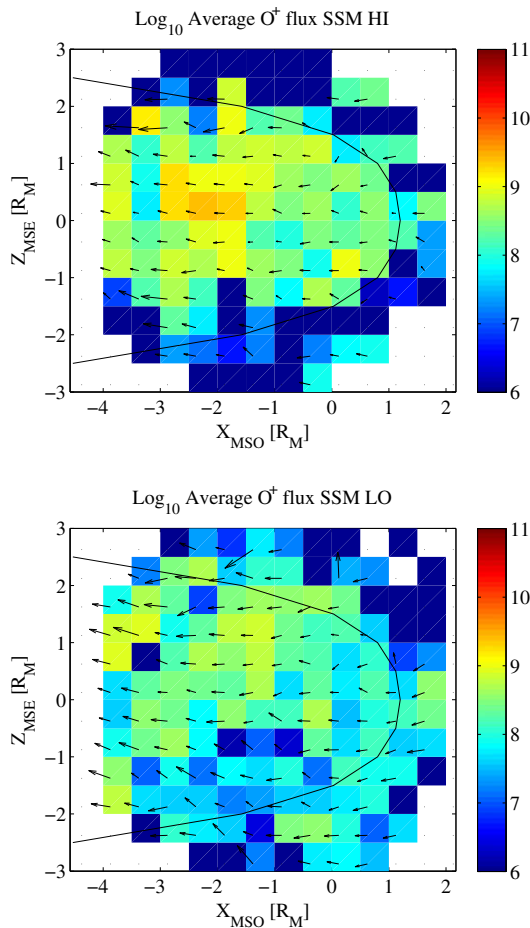
Fig. 8. The color scale shows the logarithm of average flux of O^+ [m^{-2} s^{-1}] for high subsolar magnetic field strength (upper panel) and low subsolar magnetic field strength (lower panel). The median value of 41 nT subsolar magnetic field strength was used to divide the two data sets. The axis are the same as for Fig. 1. Black arrows indicates the average ion bulk velocity, with a scale of 500 km s^{-1}/R_M.

the corresponding particle motion along the direction of the force. We also assume that a penetrating electric field is basically directed in the same direction as the external solar wind electric field. Note that the effective electric field we obtain is an electric field which the ions drift along to be accelerated, so it may be only a fraction of the total electric field giving rise to convection. As an example of such an acceleration, inertial drift in the convection electric field direction give rise to an acceleration of the particles proportional to this drift and the convection electric field, known as centrifugal acceleration in plasma physics (Northrop, 1963; Nilsson et al., 2008). The convection motion is orthogonal to the electric field so no work is done, but when another drift is added along the electric field direction work is done, leading to acceleration.

If we assume that the velocities close to Mars are biased by the instrument inability to measure low energy ions, we can set the initial bulk drift energy to 0, and the bulk drift energy of O^+ ions at 3 R_M to 1 keV. If the work is done by the solar wind electric field directed in the Z_{MSE} direction, work is done per distance traveled in the Z_{MSE} direction rather than along the tail. Assuming thus that work corresponds to ion motion in the Z_{MSE} direction but the effect of the work ends up as a bulk flow in the $-X_{MSO}$ (for example due to an initial acceleration along the electric filed and a consequent $E \times B$ drift), the effective electric field doing work on the ions is given by

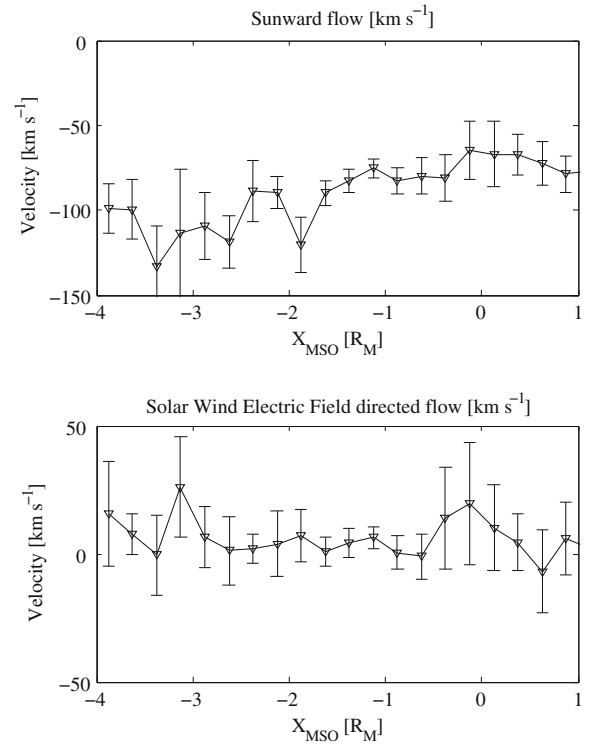$$E = \frac{\Delta W}{e \Delta l} \frac{V_x}{V_{zmse}}, \quad (1)$$

Fig. 9. The x axis shows X_{MSO} distance, positive towards the Sun, with Mars center at the origin, in units of martian radii (R_M). The y axis shows the bulk O^+ velocity [km s^{-1}] in the sunward direction (panel a) and in the direction of the solar wind electric field (panel b).

where e is the unit charge, ΔW is the change of energy in unit eV (1000 eV) per distance Δl(3 R_M), and V_x and V_{zmse} are the velocities in the tail and solar wind electric field directions respectively. Using the average of the values shown in Fig. 9 of 90 and 7 km s^{-1}, we get an effective electric field of about 1.5 mV m^{-1}. If we instead use an initial velocity of 70 km s^{-1} (consistent with Fig. 9) the resulting solar wind electric field becomes 0.8 mV m^{-1} which may be closer to expected solar wind electric fields (Dubinin et al., 2006). The effective distance traveled along the electric field direction would be about 0.2 R_M. This value is at least not unreasonably large. One may compare this with the electric field directed along the tail which would provide the same acceleration, i.e. 1000 eV/3 R_M/e = 0.1 mV m^{-1}. It should be pointed out that other possibilities exist. Energetic heavy ions observed in the tail can come from the magnetosheath region and be accelerated by the strong convection electric field there, as shown in model simulations by Fang et al. (2008). Careful comparison between observations and model predictions must be made before we can determine the precise acceleration mechanism of the ions.

It was noted in the introduction that different ion species appear to be accelerated to the same energy per charge. This creates a measurement problem, as it is easier to separate different ion species if they have both different mass and different energy, removing any problems related to cross-talk between mass channels. We would therefore like to undertake a more careful study of the details of the mass dependence of acceleration and response to solar forcing in the future. However it is clear from our data that different ion species have approximately the same energy. Fig. 10 shows the average tailward bulk velocity for three heavy ion species. The ratio between the average velocities is approximately determined by the mass ratio (16, 32 and 44 amu for O^+, O_2^+ and CO_2^+ respectively). The average ratio O^+/O_2^+ velocity is 1.5, slightly above the square root of the mass ratio of 1.4, and the average ratio
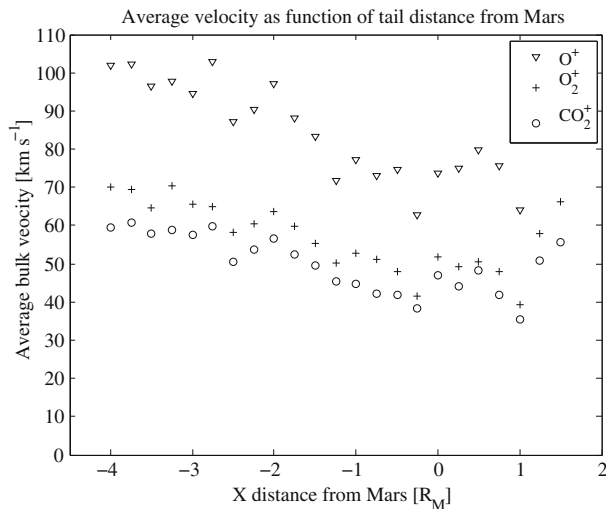
Average velocity as function of tail distance from Mars

Fig. 10. The x axis shows X_{MSO} distance, positive towards the Sun, with Mars center at the origin, in units of martian radii (R_M). The y axis shows the average bulk velocity in the sunward direction for three different species [km s^{-1}]. O$^+$ is shown with triangles, O$_2^+$ with plus signs and CO$_2^+$ with circles.

O$^+$/CO$_2^+$ velocity is 1.7, close to the same as the square root of the mass ratio of 1.65. The average bulk flow energy is thus close to the same. The data in Fig. 10 were calculated with the same automatic algorithm as used in the rest of the paper, but for a subset consisting of the orbits of manually identified ion beam events used in Carlsson et al. (2006), Carlsson et al. (2008).

4. Discussion

4.1. Solar EUV influence

From our data it is clear that we could not discern an influence on the distribution of ion fluxes around Mars or the net escape rate from the small solar EUV variations observed during the measurement period. Previous studies (Vignes et al., 2002; Trotignon et al., 2006) have found that the distribution of the planetary origin ions, i.e. the location of the MPB, is not sensitive to solar EUV flux levels, despite a large case to case variation. This is reproduced in hybrid simulations, e.g. Modolo et al. (2006). The MGS measurements of sheath-like electron spectra observed with MGS (Brain et al., 2005) does hint at an increasing trend between 2001 and 2004. This would be consistent with the MPB being closer to the planet for low solar EUV conditions. The hybrid simulation of Modolo et al. (2006) as well as the case studies reported by Lundin et al. (2008a) does indicate a significant dependence of the net escape on the solar EUV forcing. Lundin et al. (2008a) used an EUV sensitive instrument (the Neutral Particle Imager (NPI) of the ASPERA-3 instrument package) to estimate EUV fluxes locally and with high time resolution. This is likely the best method, but as the NPI instrument was designed to measure energetic neutral atoms, not EUV flux, this would require some careful analysis before an automatic algorithm suitable for statistical studies of the EUV flux through the use of the NPI instrument can be performed.

4.2. Subsolar magnetic field influence

Our data revealed two significant influences on planetary ions due to the subsolar magnetic field strength as determined from MGS measurements. First the induced magnetosphere was compressed, and the statistical border between magnetosheath and magnetosphere (defined as the region dominated by heavy ions)

was closer to the planet and sharper. This does not mean that the actual border on each occasion was sharper, but statistical fluctuation were smaller. The net escape rate was also about twice than that for low subsolar magnetic field strength for tail distances of more than 1.5 R_M from Mars center. For high subsolar magnetic fields there was a pronounced increase of the net escape with tailward distance, indicating the continuous acceleration of ions from below up to the instrument energy measurement range. Such a continuous increase was also reported in Lundin et al. (2008b), where a decrease of low energy plasma was also reported, approximately consistent with an acceleration of some of the low energy plasma. Our results indicate that it would be very well worthwhile to further study the effect of the subsolar magnetic field strength on the low energy plasma. Unfortunately there is no overlap between the improved mode of the IMA instrument allowing low energy measurements and data from the MGS spacecraft. Instead one must use the IMA measurements from the solar wind.

On average the subsolar magnetic field was about twice as strong for our high subsolar magnetic field (SSM) case as compared to the low subsolar magnetic field case. The solar wind flux was about 4 times larger for the high SSM case as compared to the low SSM case . Average proton fluxes started to fall at approximately the nominal induced magnetopause boundary for both subsolar magnetic field ranges. Presence of protons within the induced magnetosphere was much more common for the high subsolar magnetic field case, compare Fig. 1 a and b. This is true both just inside the nominal IMB, which likely indicates a change of the position of the IMB, as well as in the planet shadow. For the low SSM case the planet shadow was essentially void of any particles of solar wind origin.

These results lead to a picture where stronger subsolar magnetic field and associated solar wind fluxes compresses the induced magnetosphere. Particles of solar wind origin have some access to the induced magnetosphere, and ions of planetary origin are accelerated and removed at a higher rate. Does this fact let us distinguish between loss of ionospheric ions and loss of exospheric ions created within the region influenced by the solar wind, i.e. a classical pick up effect? In the latter case, ions should be produced where a significant heavy species exosphere exists and can be ionized by solar EUV and impact ionization from solar wind ions and electrons. The Magnetic pile-up region is generally void of solar wind origin ions, but solar wind origin electrons and solar EUV still keep creating new ions which are picked up by the flow in that region. If such ionization was the dominant process the heavy ion flow region should reflect the distribution of the exosphere. The exosphere itself will not be directly compressed by the solar wind ram pressure, so the exospheric ion production region should be fairly independent of the SSM. Therefore this compression of the heavy ion flow region indicates that we are mainly seeing the acceleration and removal of ionospheric plasma. The above reasoning is fairly idealized. In reality feedback from the solar wind to the exosphere can be expected. This feedback should mainly result in a heating of the exosphere and thus an increasing scale height. As a first approximation it therefore seems plausible that we should not get a compression of the region where heavy ions are created. The details must be investigated with models taking both ionospheric escape and exospheric ionization into account.

Mars Express does not measure the magnetic field, but as the escaping ions essentially follow the contours of the nominal IMB and associated pile up region, we expect that the ions are largely flowing with or along draped magnetic field lines but with some effect (likely finite gyro radii effects for more energetic ions) leading to an effective drift along the electric field, and a corresponding energization of the particles. A finite gyro radii effect leading to acceleration could also explain how part of the plasma can be accelerated to form the ion beams we study here, and some plas-

ma with sufficiently small gyro radius remains cold (consistent with the results of Lundin et al., 2008b). We would then expect to have a magnetized ionosphere, in order for the initially cold ionospheric plasma to be on draped field lines. This is indeed confirmed for a few cases by the pressure balance study of Dubinin et al. (2008), where it is the draped magnetic field which provides most of the pressure to balance the solar wind ram pressure in the region where the cold ionospheric plasma starts to increase to significant levels.

4.3. Solar wind electric field influence

In accordance with previous results (Fedorov et al., 2006; Carlsson et al., 2008) we found that the direction of the solar wind electric field has a profound effect on where the planetary ions are seen in the near-Mars space. The average flux density is 2 to 3 times higher in the hemisphere into which the solar wind electric field is pointed. Given the uncertainty in our estimate of the direction of the solar wind electric field the real difference could be even larger. The electric field appears to not only control the location of the ions, but also accelerate them. The ions have a progressively larger average bulk velocity the further tailward it is observed. Different ion species are accelerated to approximately the same energy, indicating acceleration by an electric field, as opposite to convection drift by an electric field which give rise to the same bulk velocity regardless of ion species. The increasing velocity with tailward distance therefore cannot solely be due to an increasing convection with tailward distance. The solar wind electric field must therefore to some extent penetrate the induced magnetosphere boundary and affect the plasma inside the induced magnetosphere. Part of the electric field appears to accelerate the plasma rather than just giving rise to a convection drift. A very rough estimate using observed average acceleration and average drift along the solar wind electric field direction provided an approximate effective acceleration electric field inside the induced magnetosphere of the order of 1 mV m^{-1} acting over an effective distance of $0.2\,R_M$. The electric field value appears somewhat large, but is similar to what Dubinin et al. (2006) deduced from a number of cases when the entire acceleration could be observed during one Mars Express passage through the induced magnetosphere. They found the effective electric field affecting the planetary ions to be of the same order of magnitude as the solar wind electric field, of the order of 1 mV m^{-1}.

Our reasoning is based on the idea that the main part of the observed escaping ions are ionospheric ions. If the ions were instead created within a region dominated by the solar wind the newly created ions would be directly affected by the solar wind electric field. The larger the electric field in the region of creation, the higher the energy of the ion. Pick-up by the solar wind flow should lead to acceleration of different mass to different energies. This is not the case for the ions observed inside the induced magnetosphere of Mars. The asymmetry in location of observed ions is also more pronounced for the high subsolar magnetic field case, when the direct interaction with the ionosphere should be strongest.

To fully understand the acceleration and outflow mechanisms we must also study the low energy plasma which can now be studied using the IMA on Mars Express. Lundin et al. (2008b) suggested, based on data taken between June 2007 and March 2008, that the colder ion component was more symmetric and not as effected by the solar wind electric field in its distribution as the more energetic ion beams. It is consistent if ions which are not effectively accelerated by the solar wind electric field are then also not strongly influenced in their distribution around the planet. This would also suggest that whereas the net result of the solar wind electric field is a net acceleration of some of the ions along the direction of the tail, there is at least no uniform low intensity elec-tric field directed along the main flow of the plasma. Then all ions would be accelerated.

5. Conclusions

A comparison between planetary origin ion flow around Mars determined from the IMA instrument on Mars Express and proxies for the solar wind conditions determined from the MGS spacecraft has been made for the period of simultaneous measurements. Because several factors are likely to influence the martian atmosphere – solar wind interaction, we chose to divide our data into two bins for each parameter, above and below median. This is to maximize the likelihood that all other independent parameters will have a similar distribution within the two data sets and thus no net contribution to any differences between the data sets. It was found that the subsolar magnetic field strength had a profound influence on the outflow of planetary origin ions around Mars. The region of outflow dominated by planetary ions was confined closer to the planet and the net escape rate within the studied energy range (above 30 eV) increased for higher subsolar magnetic field strength. At tail distances larger than $1.5\,R_M$ from Mars center the total flux was approximately doubled for a doubled subsolar magnetic field strength. We interpret the compression of the induced magnetosphere and the increase of the net outflow as evidence that the main part of the escaping plasma is of ionospheric origin, rather than recently ionized particles picked up by the magnetosheath / magnetic pile up region flow. This is also consistent with a partly magnetized ionosphere, as reported from pressure balance tests using the ASPERA and MARSIS instruments on Mars Express (Dubinin et al., 2008).

It was also found that the direction of the solar wind electric field has a strong influence on where outflowing ions in the studied energy range are found. Ions are mainly found in the hemisphere into which the solar wind electric field is pointed. The ion velocity in the antisunward direction generally increase with tail distance. The bulk flow energy is about the same for different ion species, indicating the acceleration along an electric field. The average velocity in the direction of the electric field was positive. This is consistent with some work being done by the solar wind electric field. A rough estimate indicated that if ions moved with the average velocity along the electric field direction, and with the average velocity in the tail direction, in order to gain enough energy the electric field would have to be of the order of 1 mV m^{-1}, which is roughly the same as the unshielded solar wind electric field. We interpret this as a partial penetration of the solar wind electric field into the induced magnetosphere which strongly affects the distribution of ions around Mars, and also accelerates ionospheric origin ions. Combining this with reports that some plasma remains cold throughout the tail (Lundin et al., 2008b), we suggest that finite gyro radii effects could be important. Then the net motion along the solar wind electric field would occur only for ions with a large enough gyro radius. The main motion is the usual field-aligned and $E \times B$ drift with some deviation for more energetic ions, leading to acceleration.

As a note for future research we have found that solar wind data from the IMA instrument can be used to order the data in a similar way as the subsolar magnetic field strength from the MGS spacecraft orders the data.

Finally, we compared ion distribution and net escape fluxes with a solar EUV flux proxy. The variation during our measurement period was clearly too small to discern any influence in the data.

References

Barabash, S., and the ASPERA-3 Team, 2006. The Analyzer of Space Plasmas and Energetic Atoms (ASPERA-3) for the Mars Express Mission. Space Sci. Rev. 126, 113–164.

Barabash, S., Fedorov, A., Lundin, R., Sauvaud, J.-A., 2007. Martian atmospheric erosion rates. Science 315, 501–503.

Brain, D.A., Bagenal, F., Acuña, M.H., Connerney, J.E.P., Crider, D., Mazelle, C., Mitchell, D.L., Ness, N.F., 2002. Observations of low-frequency electromagnetic plasma waves upstream from the Martian shock. J. Geophys. Res. 107 (A6). doi:10.1029/2000JA000416.

Brain, D., Halekas, J.S., Lillis, R., Mitchell, D., Lin, R., Crider, D., 2005. Variability of the altitude of the martian sheath. Geophys. Res. Lett. 32. doi:10.1029/2005GL023126.

Brain, D.A., Mitchell, D.L., Halekas, J.S., 2006. The magnetic field draping direction at Mars from April 1999 through August 2004. Icarus 182, 464–473.

Brain, D., and 26 colleagues, 2008. A Comparison of Global Models for the Solar Wind Interaction with Mars. Icarus, 206(1), 139–151.

Carlsson, E., and 47 colleagues, 2006. Mass composition of the escaping plasma at Mars. Icarus 182, 320–328.

Carlsson, E., Brain, D., Luhmann, J., Barabash, S., Grigoriev, A., Nilsson, H., Lundin, R., 2008. Influence of IMF draping direction and crustal magnetic field location on Martian ion beams. Planet. Space Sci. 56, 863–867.

Dubinin, E.M., Lundin, R., Norberg, O., Pissarenko, N., 1993. Ion acceleration in the Martian tail: The Phobos observations. J. Geophys. Res. 98, 3991–3997.

Dubinin, E., and 12 colleagues, 2006. Electric fields within the martian magnetosphere and ion extraction: ASPERA-3 observations. Icarus 182, 337–342.

Dubinin, E., and 11 colleagues, 2008. Structure and dynamics of the solar wind/ionosphere interface on Mars: MEX-ASPERA-3 and MEX-MARSIS observations. Geophys. Res. Lett. 35. doi:10.1029/2008GL033730.

Fang, X., Liemohn, M.W., Nagy, A.F., Ma, Y., De Zeeuv, D.L., Kozyra, J.U., Zurbuchen, T.H., 2008. Pickup oxygen ion velocity space and spatial distribution around Mars. J. Geophys. Res. 113, A02210. doi:10.1029/2007JA012736.

Fedorov, A., Budnik, E., Sauvaud, J.-A., Mazelle, C., Barabash, S., Lundin, R., Acũna, M., Holmström, M., Grigoriev, A., Yamauchi, M., 2006. Structure of the Martian wake. Icarus 182, 329–336.

Futaana, Y., and 53 colleagues, 2006. Mars Express and Venus Express multi-point observations of geoeffective solar flare events in December 2006. Planet. Space Sci. 56, 873–880.

Kallio, E., 1996. An empirical model of the solar wind flow around Mars. J. Geophys. Res. 101, 11133–11148.

Luhmann, J.G., 1990. The solar wind interaction with unmagnetized planets—A tutorial. In: Geophysical Monograph Series, vol. 58. American Geophysical Union, Washington, DC, pp. 401–411.

Lundin, R., Zakharov, A., Pellinen, R., Barabasj, S.W., Borg, H., Dubinin, E.M., Hultqvist, B., Koskinen, H., Liede, I., Pissarenko, N., 1990. ASPERA/Phobos measurements of the ion outflow from the Martian ionosphere. Geophys. Res. Lett. 17, 873–876.

Lundin, R., Barabash, S., Fedorov, A., Holmström, M., Nilsson, H., Sauvaud, J.-A., Yamauchi, M., 2008a. Solar forcing and planetary ion escape from Mars. Geophys. Res. Lett. 35. doi:10.1029/2007GL032884.

Lundin, R., Barabash, S., Holmström, M., Nilsson, H., Yamauchi, M., Fraenz, M., Dubinin, E.M., 2008b. A comet-like escape of ionospheric plasma from Mars. Geophys. Res. Lett. 35. doi:10.1029/2008GL034811.

Mitchell, D., Lin, R., Mazelle, C., Rème, H., Cloutier, P., Connerney, J., Acuna, M., Ness, N., 2001. Probing Mars' crustal magnetic field and ionosphere with the MGS electron reflectometer. J. Geophys. Res. 106 (E10), 23419–23427.

Modolo, R., Chanteur, G.M., Dubinin, E., Matthews, A.P., 2006. Simulated solar wind plasma interaction with the Martian exosphere: Influence of the solar EUV flux on the bow shock and the magnetic pile-up boundary. Ann. Geophys. 24, 3403–3410.

Nilsson, H., and 11 colleagues, 2006. Investigation of the influence of magnetic anomalies on ion distributions at mars. Space Sci. Rev. 126, 355–372.

Nilsson, H., and 14 colleagues, 2008. An assessment of the role of the centrifugal acceleration mechanism in high altitude polar cap oxygen ion outflow Ann. Geophys. 26, 145–157.

Northrop, T.G., 1963. The Adiabatic Motion of Charged Particles. Interscience Publishers, NY.

Sauer, K., Bogdanov, A., Baumgärtel, K., 1994. Evidence of an ion composition boundary (protonopause) in bi-ion fluid simulations of solar wind mass loading. Geophys. Res. Lett. 21 (20), 2255–2258.

Trotignon, J.G., Mazelle, C., Bertucci, C., Acuna, M.H., 2006. Martian shock and magnetic pile-up boundary positions and shapes determined from the Phobos 2 and Mars Global Surveyor data sets. Planet. Space Sci. 54, 357–369.

Verigin, M.I., and 16 colleagues, 1991. Ions of planetary origin in the martian magnetosphere (Phobos 2/taus experiment). Planet. Space Sci. 39, 131–137.

Vignes, D., Acuña, M.H., Connerney, J.E.P., Rème, H., Mazelle, C., 2002. Factors controlling the location of the Bow Shock at Mars. Geophys. Res. Lett. 29. doi:10.1029/2001GL014513.